AD-A134 213 INTERACTIONS OF AIRFOILS WITH GUSTS AND CONCENTRATED VORTICES IN UNSTEADY TRANSONIC FLOW(U) NATIONAL AERONAUTICS AND SPACE ADMINISTRATION MOFFETT FIELD C.. 1/1

UNCLASSIFIED W J MCCROSKEY ET AL. 1983 F/G 20/4 NL

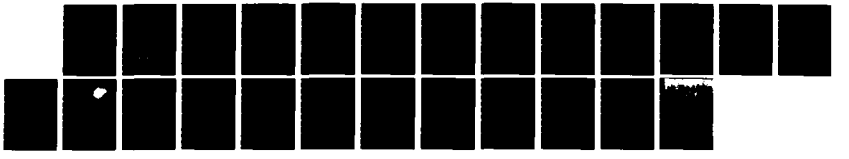

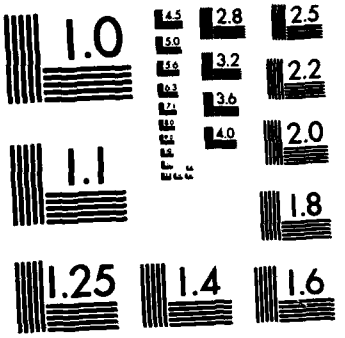

AIAA'83

(1)

AIAA-83-1691

Interactions of Airfoils with Gusts and Concentrated Vortices in Unsteady Transonic Flow

W. J. McCroskey and P.M. Goorjian
NASA Ames Research Center
Moffett Field, CA

AD-A134 123

AIAA 16th Fluid and Plasma Dynamics Conference

July 12-14, 1983
Danvers, Massachusetts

INTERACTIONS OF AIRFOILS WITH GUSTS AND CONCENTRATED VORTICES IN UNSTEADY TRANSONIC FLOW

W. J. McCroskey* and P. M. Goorjian†
NASA Ames Research Center, Moffett Field, California

Abstract

Unsteady interactions of concentrated vortices and distributed free-stream gusts with a stationary airfoil have been analyzed in two-dimensional transonic flow. A simple method of introducing such disturbances has been implemented numerically in the well-known transonic small-disturbance code LTRAN2, and calculations have been performed for two important classes of current aerodynamic problems. The first, which demonstrates many of the essential features of the interactions between helicopter rotor blades and their trailing-vortex wakes, is that of a discrete potential vortex convecting past an airfoil. The second is the response of a transonic airfoil to a transverse periodic gust, with and without the alleviation that can be achieved by the proper active control motion of a trailing-edge flap. In both cases, unsteady effects are found to play important roles in the shock-wave motion, in the overall flow-field development, and consequently, in the air loads on the airfoil.

Nomenclature

A = amplitude ratio, defined following Eq. (14)

a = vortex core radius

B = $M_\infty \varepsilon^{-2/3}$

C_1 = $(1 - M_\infty)\varepsilon^{-2/3}$

C_2 = $-(1 + \gamma)M_\infty^m$

C_L = lift coefficient

C_M = moment coefficient

C_p = pressure coefficient

c = airfoil chord, m

D_x = difference operator, defined following Eq. (3)

f = defined following Eq. (3)

i,j = indices in x- and y-directions, respectively; also unit vectors in x- and y-directions

k = reduced frequency, $\omega c/u_\infty$

M = Mach number

m = exponent in Eq. (1); also dummy time index

n = time index

$\vec{q}$ = nondimensional velocity

$\vec{q}_v$ = velocity induced by the vortex

$\vec{q}_1$ = velocity at the location of the vortex, excluding $\vec{q}_v$

$\vec{r}_0$ = initial position of the vortex

$\vec{r}_1$ = instantaneous position of the vortex

$t,\hat{t}$ = dimensionless and dimensional time, respectively, sec

U_∞ = free-stream velocity, m/sec

u,v = dimensionless velocities in the x- and y-directions, respectively

u_v,v_v = velocities induced by the vortex

v_G = gust velocity

x,y = directional coordinates

x_0,y_0 = initial position of the vortex

x_1,y_1 = instantaneous position of the vortex

α = angle of attack, deg

γ = ratio of specific heats

Γ = strength of the vortex

Δ_x = difference operator, defined following Eq. (3)

δ = difference operators, defined following Eq. (3)

δ_F = flap deflection, deg

ε = airfoil thickness ratio

θ,Θ = phase angles, defined following Eq. (14)

Λ = sweep angle, Fig. 1

ϕ,Φ = disturbance potentials, with and without the vortex, respectively

ω = frequency of oscillation, rad/sec

I. Introduction

The unsteady interaction of concentrated vortices, gusts, and related vortical disturbances with lifting surfaces can be important for a variety of fluid-dynamic devices, such as maneuvering aircraft and missiles, helicopter rotor blades, and turbomachinery. Frequently, these interactions alter the flow field significantly, with consequent changes in aerodynamic loading, aeroelastic behavior, and acoustic characteristics.

*Senior Staff Scientist, U.S. Army Aeromechanics Laboratory and NASA Thermo- and Gas-Dynamics Division. Associate Fellow AIAA.

†Research Scientist, NASA Applied Computational Aerodynamics Branch. Member AIAA.

These phenomena can be especially acute in the transonic-flow regime, where shock-wave positions and strengths are sensitive to small changes in the flow parameters. At the same time, the development of predictive techniques for vortex flows in this difficult nonlinear regime has not kept pace with the evolution of engineering methods for flows at either higher or lower Mach numbers; see, for example, the recent collection of papers in Ref. 1.

A particularly complex practical example of this type is the passage of helicopter rotor blades through their vortical wakes at low and moderate flight speeds. The blade tips, which trail strong, concentrated tip vortices, trace out prolate cycloidal paths in space, leading to a variety of possible blade-vortex interactions. The generic problem, sketched in Fig. 1, can be viewed as an unsteady, three-dimensional close encounter of a curved-line vortex, at an arbitrary intersection angle Λ, with a high-aspect-ratio lifting surface that is executing combined rotational and translational motion at transonic speeds. The limiting cases for $\Lambda = 0°$ and $90°$ are illustrated in Figs. 2a and 2b, respectively; the former is essentially two-dimensional but unsteady, whereas the latter can be considered as steady but highly three-dimensional. The recent paper by George and Chang[2] is recommended for more discussion of these representations and their aeroacoustic implications.

This investigation was motivated primarily by the situation depicted in Fig. 2a, as a first step in developing practical methods for predicting general three-dimensional, unsteady interactions. In this vein, the following section describes the basic formulation of the problem and the modification of an existing, efficient, and well-exercised, two-dimensional computer code[3,4] to treat this class of unsteady, transonic vortex-interaction problems. However, the manner in which the vortex is introduced readily lends itself to other types of convected flow-field disturbances, such as gusts, and this extension can easily be combined with the inherent capability of the original code to treat airfoils with moving control surfaces. Consequently, the method has also been applied to cases of distributed sinusoidal gusts in the free stream and to the alleviation of such gusts by means of control-surface deflections, in addition to the concentrated vortex-airfoil interaction problem. Results for representative examples of each of these problems are discussed and analyzed in subsequent sections of the paper.

II. Numerical Formulation

The transonic small-disturbance approximation to the velocity-potential equation was chosen for the present investigation, as a fruitful compromise between simplicity, computational efficiency, and accuracy. Viscous effects are thus ignored, and the results are also acknowledged to be inaccurate in the immediate vicinity of the leading edge. However, most of the qualitative features of the interaction phenomena and considerable quantitative information can be obtained within the scope of this approximation. Also, useful solutions can be calculated using the basic algorithm and much of the original coding of an established numerical program called LTRAN2 (Refs. 3 and 4). However, the special features of the vortex-and-gust-interaction problems considered in this paper did require several additions to the basic equations and boundary conditions and, hence, some significant modifications to the code LTRAN2, as outlined below.

A. Governing Equation and Numerical Algorithm

The unsteady, transonic small-disturbance equation for the velocity potential can be written in the following form[3,4]:

$$B\Phi_{tt} + 2B\Phi_{xt} = \frac{\partial}{\partial x}\left[(C_1 + C_2\Phi_x)\Phi_x\right] + \Phi_{yy} \qquad (1)$$

where

$$B = M_\infty^2 \varepsilon^{-2/3}$$

$$C_1 = (1 - M_\infty^2)\varepsilon^{-2/3}$$

$$C_2 = -(\gamma + 1)M_\infty^m$$

$$\nabla\Phi = \vec{q} - 1$$

Here ε is the airfoil thickness ratio, and the dimensionless quantities x, y, t, $\vec{q}$, and Φ are scaled by c, $c\varepsilon^{-1/3}$, c/U_∞, U_∞, and $c\varepsilon^{2/3}U_\infty$, respectively. In the LTRAN2 codes, the exponent m appearing in the coefficient C_2 of the nonlinear term $\Phi_x\Phi_{xx}$ can be set to the value 2 for the so-called Spreiter,[5] or nonconservative, scaling, or allowed to vary as an empirical function of local and free-stream Mach numbers.[3] In the latter case, Eq. (1) closely approximates the formal small-disturbance limit of the conservative form of the full-potential equation.[6] Inclusion of the various additional nonlinear terms, for example, $\Phi_t\Phi_{xx}$, $\Phi_x\Phi_{xt}$, which arise in sundry derivations of the small-disturbance equations, does not seem to be warranted at this stage.

On the other hand, the term $B\Phi_{tt}$, which was dropped in previous versions of the code LTRAN2, should be included here, because the nondimensional time scale of the vortex or gust interaction, $U_\infty\hat{t}/c$, may be of the order of unity. This has been accomplished by adding Φ_{tt} contributions to both the x- and y-sweeps of the alternating-direction-implicit (ADI) scheme in the code LTRAN2-HI (Ref. 4); in addition, the more robust monotone type-dependent differencing switch of Goorjian and Van Buskirk[7] was substituted for the standard Murman-Cole switch in LTRAN2-HI. Thus, in the present case the solution is advanced from time-level n to $n + 1$ as follows:

x-sweep:

$$\frac{B}{(\Delta t)^2}(\phi^* - 2\phi^n + \phi^{n-1}) + \frac{2B}{\Delta t}\delta_x(\phi^* - \phi^n) = D_x f + \delta_{yy}\phi \qquad (2)$$

y-sweep:

$$\frac{B}{(\Delta t)^2}(\phi^{n+1} - \phi^*) + \frac{2B}{\Delta t}\delta_x(\phi^{n+1} - \phi^*) = \frac{1}{2}\delta_{yy}(\phi^{n+1} - \phi^n) \qquad (3)$$

Here ϕ is understood to be subscripted with i for the x-direction and j for the y-direction,

and ϕ^* is the intermediate value of the unknown potential at the end of the predictor step, Eq. (2). Following approximately the notation of Refs. 3 and 7,

$$D_x f = \vec{\Delta}_x \tilde{f} + \overleftarrow{\Delta}_x \hat{f}$$

$$\tilde{f}_{i-1/2,j} = \frac{1}{2}\left[C_1 \tilde{u} + (C_1 + 2C_2 \tilde{u}) \vec{\delta}_x \phi^*_{i,j}\right]$$

$$\hat{f}_{i-1/2,j} = \frac{1}{2}\left[C_1 \hat{u} + (C_1 + 2C_2 \hat{u}) \overleftarrow{\delta}_x \phi^*_{i,j}\right]$$

$$\vec{\Delta}_x \tilde{f} = \frac{\tilde{f}_{i+1/2,j} - \hat{f}_{i-1/2,j}}{\frac{1}{2}(x_{i+1} - x_{i-1})}$$

$$\overleftarrow{\Delta}_x \hat{f} = \frac{\hat{f}_{i-1/2,j} - \hat{f}_{i-3/2,j}}{\frac{1}{2}(x_{i+1} - x_{i-1})}$$

$$\overleftarrow{\delta}_x \phi_{i,j} = \frac{\phi_{i,j} - \phi_{i-1,j}}{x_i - x_{i-1}} \; ; \quad \delta_x \phi_{i,j} = \frac{\phi_{i,j} - \phi_{i-1,j}}{\frac{1}{2}(x_{i+1} - x_{i-1})}$$

$$\tilde{u} = \min(\bar{u},\, u_{i-1/2,j})$$

$$\hat{u} = \max(\bar{u},\, u_{i-1/2,j})$$

$$\bar{u} = -C_1/C_2$$

$$u_{i-1/2,j} = \overleftarrow{\delta}_x \phi^n_{i,j}$$

$$\delta_{yy}\phi_{i,j} = 2[(\phi_{i,j+1} - \phi_{i,j})/(y_{j+1} - y_j) - (\phi_{i,j} - \phi_{i,j-1})/(y_j - y_{j-1})]/(y_{j+1} - y_{j-1})$$

It should be mentioned that the evaluation of the term ϕ_{yy} in this new scheme is only first-order accurate in both time and space, whereas the basic LTRAN2 algorithm is second-order accurate in time and first-order accurate in space. For the applications considered in this paper, however, this reduction in theoretical accuracy is inconsequential.

Another aspect of the present method is that by including a first approximation to ϕ_{tt} in the x-sweep, the solution at time-level $n - 1$, ϕ^{n-1}, does not appear in the subsequent y-sweep. Consequently, at any given step in the calculation, only two two-dimensional arrays are required in the computer memory to store the necessary intermediate values of the solution. This characteristic enabled us to revise the LTRAN2-HI code to solve Eqs. (2) and (3) without having to store any additional large data arrays. The resultant savings in storage requirements can be an important advantage for computer systems with limited memory capacity, and it would be even more so in three-dimensional problems.

Figure 3 shows the results of including the ϕ_{tt} term for a linear test case, in comparison with the results obtained with the original code LTRAN2 (Ref. 3) and with the subsequent refinements of Hessenius and Goorjian[4] in LTRAN2-HI. Particularly noteworthy is the improvement in the pitching moment results, which were a problem before.

B. Introduction of Nonuniformities in the Free Stream

A concentrated potential vortex can be introduced into an irrotational flow field in either of two different ways, as illustrated schematically in Fig. 4. The first, which we shall call the branch-cut method, is due to Caradonna[8] and Caradonna et al.[9] and is a straightforward extension of classical potential theory for lifting bodies. As indicated in Fig. 4a, a branch cut is introduced between the vortex and the outer boundary of the flow field, and a jump in potential equal to the strength of the vortex is prescribed across this branch cut. The flow remains irrotational, of course, outside the airfoil and vortex branch cuts. If the vortex moves through the flow field, the branch cut moves accordingly.

In finite-difference implementations of the branch-cut method, the natural choice is to make the vortex and airfoil cuts coincident with grid lines. Then, as the vortex moves through the flow field, the logic of the code must move the branch cut to new grid lines; but this must be done smoothly to avoid introducing artificial disturbances into the solution domain. One such smoothing method was recently demonstrated by Murman and Stremel,[10] who distributed individual point vortices over neighboring grid points using Baker's vortex-in-cell area-weighting and bilinear-interpolation scheme.[11]

The second approach, which we adopt here and call the prescribed-disturbance method, evolved in private discussions with John Steinhoff, who recently illustrated the method in Ref. 12 for the steady, three-dimensional, full-potential equation and a wing-vortex interaction problem. The basic idea, indicated schematically in Fig. 4b, also parallels certain aspects of Goldstein's[13] and Kerschen and Myers'[14] aeroacoustic extensions of the so-called rapid-distortion theory of turbulence, using the linear wave equation. Here the essential point is that, although Eq. (1) is nonlinear and independent solutions are not superposable, the velocity field can still be split into three parts: 1) the (uniform) free stream, 2) a prescribed disturbance, $\vec{q}_v$, for example, gusts, concentrated vortices, etc., and 3) the disturbance potential $\nabla\phi$ due to the airfoil itself. That is,

$$\vec{q} = 1 + \vec{q}_v + \nabla\phi \tag{4}$$

If Eq. (4) is substituted into the governing equation(s), a new and more complicated equation will result, unless the original equation was linear. Moreover, the prescribed disturbance at each time-step or iteration may turn out to depend on the solution of the governing equation at the previous time step or iteration. However, it may also turn out that a given solution technique or algorithm that has been developed for the original governing equation will work equally well for the new, more complicated equation. That is the case here, which is particularly straightforward in the small-disturbance limit.

For convenience and for purposes of illustration, $\vec{q}_v = \vec{i}u_v + \vec{j}v_v$ is chosen to satisfy the linearized version of Eq. (1) (i.e., with $C_2 = 0$). Then substituting Eq. (4) into Eq. (1) and

subtracting out the linear terms gives the following equation for the unknown disturbance potential ϕ:

$$B\phi_{tt} + 2B\phi_{xt} = C_1\phi_{xx} + C_2 \frac{\partial}{\partial x} (\phi_x + u_v)^2 + \phi_{yy} \tag{5}$$

The same substitution is also made in the original boundary conditions, which were 1) flow tangency on the body, 2) no disturbances at $x \to -\infty$ and $y \to \pm\infty$, and 3) $C_p = 0$ at $x \to +\infty$. The new small-disturbance boundary condition on the body, $y_b = F(x,t)$, becomes

$$\phi_y(x, y \to 0) = F_x + F_t - v_v \tag{6}$$

The wake condition of zero pressure jump across the airfoil branch-cut remains unchanged, that is,

$$(\Gamma_x + \Gamma_t)_w = 0 \tag{7}$$

With the respecification of the appropriate boundary conditions at the outer boundaries of the computational domain, Eqs. (5)-(7) result in a new well-posed problem for ϕ that can be solved by the same basic algorithm as before. Equations (2) and (3) read the same, except it is understood that Φ is replaced by ϕ, the various u, $\tilde{u}$, $\hat{u}$, etc. are replaced everywhere by $(u + u_v)$, etc., and the nonlinear term becomes

$$D_x f = \vec{\Delta}_x \tilde{f}_{i-1/2,j} + \vec{\Delta}_x \hat{f}_{i-1/2,j} + \frac{1}{2} C_2 \delta_x [(\delta_x \phi^n + u_v) u_v] \tag{8}$$

In this derivation, the strength and structure of the prescribed disturbance are implicitly assumed to be unaltered by the presence of the airfoil, and it is convected through the flow field at the velocity of the local fluid elements. Then, for the particular case in which the imposed disturbance is a concentrated, moving potential vortex, its disturbance field and position in scaled variables are given by

$$u_v = -\frac{\Gamma}{2\pi\varepsilon} \left[\frac{y - y_1}{(x - x_1)^2 + (y - y_1)^2 \varepsilon^{-2/3}} \right] \tag{9}$$

$$v_v = \frac{\Gamma}{2\pi\varepsilon} \left[\frac{y - y_1}{(x - x_1)^2 + (y - y_1)^2 \varepsilon^{-2/3}} \right] \tag{10}$$

$$\vec{f}_1 = \vec{f}_0 + \int_{t_0}^{t} \vec{q}_1 \, dt \tag{11a}$$

$$\approx \vec{f}_0 + \sum_{m=1}^{n} \vec{q}_{1_m} \Delta t \tag{11b}$$

where $\vec{f}_1 = (x_1, y_1)$ is the instantaneous position of the vortex; $\vec{f}_0$ is the original position of the vortex when the calculation is initiated; Γ is the vortex strength, normalized by c and U_∞; and $\vec{q}_1 = (u_1, v_1)$ is the velocity at the vortex location $\vec{f}_1$, obtained from the numerical solution of Eq. (5) at time-level m. We note in passing that although such a vortex contributes first-order terms in Eqs. (5) and (6), its net contribution to the small-disturbance Bernoulli equation for C_p is second order, and hence negligible.

In contrast with the branch-cut method, we see that the present approach introduces additional nonlinear terms into the governing equation and into the boundary conditions on the airfoil, but that the moving branch-cut logic of the former method is effectively replaced by the simple expression of Eq. (11b). In addition, the prescribed disturbance need not be restricted to the form of Eqs. (9) and (10); for example, a vortex with a viscous core and finite velocity at its origin could also be specified. In fact, this was found to be necessary for most of the examples considered, as explained in Sec. IIC.

The prescribed-disturbance method can also be extended to much more general cases of vortical or other disturbances. This is especially simple in the small-disturbance limit, where most, or perhaps all, of the resulting cross terms will be negligible and the coding modifications will be minimal. Typical practical examples include small-amplitude atmospheric gusts, of either the sharp-edged or traveling-wave type, which heretofore have only been treated with linear analyses. Furthermore, if the gust is uniform in the direction normal to its disturbance velocity, its effect enters only through the airfoil boundary condition, Eq. (6), if it is a vertical gust, or through C_p and the nonlinear term $(\phi_x + u_G)^2$ in Eq. (5) if it is a horizontal gust. Examples of the former type are given in Sec. IV, with and without accompanying control-surface deflections.

C. Effects of Secondary Numerical Parameters

Calculations were performed with both $m = f(M, M_\infty)$ and with $m = 2$ in Eq. (1), and with certain other parameters in the numerical code that were chosen somewhat arbitrarily. These included the step size Δt; the number of grid points and their distribution; and the value of x_0 where the vortex was initially introduced and the radius a of the core of the vortex, in the airfoil-vortex interaction examples.

The effect of the exponent m in Eq. (1) was found to be merely what would be expected from the steady case for Spreiter scaling versus fully conservative scaling. That is, the former scaling tended to produce weaker shock waves and smaller supersonic zones. However, the basic qualitative effects of the airfoil-vortex or airfoil-gust interactions were unaffected.

Most of the calculations performed in this investigation were done with the standard LTRAN2 grid of 113 points in the x-direction and 97 in the y-direction, with smooth stretching in both directions to outer boundaries 200 chord lengths away. However, finer x-grids of up to 186 points were found to be necessary for adequate resolution of the pressure-wave propagation in some of the airfoil-vortex interaction cases with the NACA 64A006 airfoil. These finer grids were also required for the oscillating-airfoil and sinusoidal-gust cases at reduced frequencies greater than about two, where the computed results began to deviate from linear theory otherwise. The computation times were dependent on the number of grid points; CPU times were approximately 1.5×10^{-5} sec per grid point per time step on the Cray 1-S

computer at Ames Research Center (or between 1 and 5 min per case), and about twice this on the CDC 7600 machine.

The calculations of pitching oscillations and gust responses were normally done with 240 time steps per cycle over 5 or 6 cycles of oscillation, after it was established that the solutions were independent of Δt for more than about 180 steps per cycle. Most of the airfoil-vortex interaction cases were performed with $\Delta t = 0.02$. The accuracy of the nonlinear results began to degrade for $\Delta t = 0.05$, and spurious oscillations in the solutions sometimes appeared for $\Delta t < 0.02$.

The results in Sec. III show that the vortex began to influence the pressure distribution on the airfoil, although weakly, when it was very far upstream. For computational economy, therefore, the vortex was normally introduced at 7 to 10 chord lengths upstream of the leading edge, and then its strength was increased linearly with time from zero initially to the full value after 1 chord length of travel. Solutions obtained with $x_0 = -7$, -10, and -20 were found to be virtually the same by the time the vortex was within 3 chord lengths of the leading edge and the pressures on the airfoil began to vary rapidly.

Numerical instability problems were encountered early in the investigation when the potential vortex of Eqs. (9) and (10) was employed in nonlinear calculations. These difficulties were traced to excessive values of u_v and its x-derivative; consequently, a vortex with a finite core velocity was introduced, having an induced velocity field given by

$$|q_v| = \frac{\Gamma}{2\pi\varepsilon r}\left(1 - e^{-r^2/a^2}\right) \qquad (12)$$

where

$$r^2 = (x - x_1)^2 + (y - y_1)^2\varepsilon^{-2/3}$$

This velocity field is illustrated in Fig. 5. It is noteworthy that q_v is very nearly equal to the ideal-vortex value of Eqs. (9) and (10) for $r > 2a$. Therefore, the predominant effect of a is felt only very locally in the flow field, and there only through the nonlinear term $(\phi_x + u_v)^2$, in the small-disturbance limit of the present study. Test calculations showed the solutions to be essentially independent of a for the range $0.02 < a < 0.07$; the value 0.05 was used for the results presented in Sec. III. The resolution of this numerical difficulty by means of a vortex with a core may have implications for future work using the branch-cut method, as well.

III. Airfoil-Vortex Interactions

A. Results for the NACA 0012 Airfoil

The problem of a concentrated potential vortex convecting past a stationary airfoil is indicated schematically in Fig. 2a. Parathasarathy[15] and Chow and Huang[16] have found incompressible solutions using conformal mapping techniques for this general case. As discussed in Sec. II, this problem was first treated in the transonic case by Caradonna et al.,[9] using the branch-cut method for introducing the vortex, the small-disturbance equations with Spreiter scaling, and a somewhat different ADI algorithm. Accordingly, the present code was first checked out for the cases published in Ref. 9, for the NACA 0012 airfoil at $M_\infty = 0.8$. Some representative examples are given in Figs. 6 and 7. In this particular case, the vortex is prescribed to move at free-stream velocity along the path $y_1 = \text{constant}$, and $x_1 = x_0 + U_\infty \hat{t}/c$, following Ref. 9. The effect of this approximation is examined in Sec. IIIC.

Figure 6 shows the pressure distribution on the airfoil at several stages of the vortex passage. The agreement between the two methods is satisfactory, except for the time when the vortex is beneath the midchord of the airfoil. It should be mentioned that for this particular set of conditions, the interaction is quite severe in terms of the small-disturbance approximation. The numerical solutions seem to be marginally stable, depending on the mesh distribution, on Δt, and on the vortex core radius. Nevertheless, the two independent sets of results illustrate most of the essential features of the airfoil-vortex interaction.

In a very general sense, the initial development of the pressure difference across the airfoil resembles the expected response of the flow to a decrease in angle of attack; that is, the vortex induces a spacially varying "downwash," or negative v-velocity perturbation, in the flow approaching the airfoil. However, the effect is much larger on the lower surface than on the upper, a result of nonlinear effects. Also, the actual shape of the pressure distributions, the shock-wave strengths and positions, and the time history of the airfoil pressures are quite different, even qualitatively, from the results for airfoil oscillations, or from the results for the sinusoidal gusts considered in Sec. IV.

Finally, after the vortex passes behind the airfoil, its induced field becomes an "upwash" distribution of vertical velocity. The qualitative effect of this is, very approximately, the inverse of the behavior when the vortex is upstream of the airfoil. However, the return of the flow around the airfoil to the original state is extremely slow, even though the lingering effects are much weaker.

B. Results for the NACA 64A006 Airfoil

This airfoil, which has been used in numerous numerical and experimental studies, is not only thinner than the NACA 0012 section, but has a significantly smaller leading-edge radius as well. Therefore, it might be expected to be more sensitive to the vortex-induced downwash than the NACA 0012 profile.

Figures 8-11 show the results for an unsteady case with $m = 2$ and with the same vortex strength and initial value of y_{v_0} as in the previous example, but at $M_\infty = 0.85$ and with a force-free trajectory given by Eq. (11). Here the airfoil incidence is zero, and the dramatic differences between C_p on the upper and lower surface are due solely to the vortex interaction. As before, the vortex distorts the flow on the lower surface of the airfoil more than on the upper.

As in the previous case, the effect of the vortex on the airfoil flow field is felt for vortex positions many chord lengths upstream and downstream of the origin. However, the most rapid and dramatic changes in the airfoil pressure distributions occur when the vortex is within 1 or 2 chord lengths of the airfoil. For this particular airfoil, these principal variations in C_p have two other distinct stages of pressure fluctuations superimposed upon them. The first is the rapid development of a large suction peak near the lower leading edge as the vortex approaches. This is followed soon thereafter by an even more rapid increase in C_p, that is, by a rapid compression. As noted by George and Chang,[2] a compression wave seems to leave the airfoil at this point and propagate into the oncoming flow. The inverse of this phenomenon occurs in the upper-surface leading-edge region, that is, a local compression followed by an expansion. However, the magnitude and rate of change of the fluctuating pressure there is considerably less, and an expansion wave does not seem to propagate forward.

The second pattern of moving pressure waves occurs some time after the vortex passes downstream of the trailing edge. The shock wave on the lower surface begins to creep forward, weakening as it moves. Eventually a weak compression wave moves forward, ahead of the shock wave, but it essentially vanishes before it reaches the leading edge. This lower surface behavior resembles the so-called type B unsteady shock-wave motion of Tijdeman,[17] as noted by George and Chang.[2] During this time, the upper-surface shock wave gradually weakens, as the flow returns slowly toward the initial undisturbed state. Although they move significantly and change in strength, the primary shock waves on both the upper and lower surfaces remain attached to their respective sides of the airfoil throughout the vortex-encounter events.

Figures 12 and 13 show the same type of results as Figs. 8 and 9, but for a lower free-stream Mach number. This is the airfoil and Mach number for which the Tijdeman type C shock-wave motion was calculated by Ballhaus and Goorjian[3] for an oscillating flap. A weak type C behavior on the lower surface is evident here as well, but the compression wave essentially vanishes before reaching the leading edge.

C. Effects of Various Approximations

A number of test cases were run for the preceding flow conditions, with various terms deleted one at a time from the basic equations. The results of this numerical experimentation are summarized in Figs. 14-19, which show the time-history of the lift and two instantaneous pressure distributions for each case.

Figure 14 shows the effect of neglecting the ϕ_{tt} term; as reported by George and Chang,[2] this term does not seem to be as important as was originally thought. However, it was found to have somewhat of a stabilizing effect on calculations that were marginally stable.

Figures 15 and 16 show the effect of neglecting the horizontal and vertical components, respectively, of the vortex-induced velocity. It is clear from these two figures that the latter is the most important, at least for this particular Mach number and airfoil section. This result indicates that the approximation of George and Chang[2] in neglecting u_v was not too serious. However, in comparison with the results in Figs. 8-11, the perturbations in the lower-surface pressures in the leading-edge region are too large when u_v is neglected.

Figure 17 shows the effect of specifying that the vortex move along a straight line, $y_1 = y_0$ and $x_1 = x_0 + U_\infty \hat{t}/c$, rather than allowing it to move on the force-free path given by Eq. (11). In the latter instance, the vortex is displaced farther from the airfoil, and its effect on the flow field around the airfoil weakens as a result.

Finally, Figs. 18 and 19 show the effect of neglecting the nonlinear term altogether, that is, a linear calculation. The overall lift and moment are not too different from the values calculated using the full nonlinear formulation, but the time history of the leading-edge pressures shows much less rapid fluctuations. The changes in the upper and lower pressures from the initial values without the vortex present are, of course, exactly equal and opposite for this case.

IV. Airfoil-Gust Interactions

The modifications outlined in Sec. II make it possible to calculate the effects of gusts in the free stream. This is illustrated for the particular case of the classical longitudinally traveling, sinusoidal gust of vertical velocity,

$$v_G = w_1 \sin[\omega \hat{t} - k_G(x - 1/2)] \qquad (13)$$

This expression for v_G replaces v_v in the boundary condition on the airfoil, Eq. (6). There is no u-component of velocity for this particular type of gust. Also, the distortion of the gust field by the presence of the airfoil, as treated by Kerschen and Myers[14] in the linear case, is ignored.

Figure 20 shows linear results obtained with the present code for the Sears lift function[18] in comparison with the compressible results of Graham[19] for low- and high-subsonic Mach numbers, over a wide range of reduced frequencies. As in Fig. 3, $k = \omega c/U_\infty$ is based on the chord length, and here k_G is inversely proportional to the wavelength of the gust. The agreement is comparable to that shown in Fig. 3 for pitching oscillations.

A. Nonlinear Gust Response

Figure 21 shows the distortions in the pressure distribution on an NACA 0012 airfoil in transonic flow due to a sinusoidal gust. In this case, the fluctuations in the solution are antisymmetric on the upper and lower surfaces of the airfoil. The steady and first-harmonic content of these fluctuations are compared with linear results in Figs. 22 and 23 at $M_\infty = 0.80$ and $k = 0.2$ and 2.0, respectively. The peak in the nonlinear results near midchord is a direct result of the motion of the shock wave; see, for instance, Ref. 20. This effect attenuates with increasing reduced frequency, similar to the trends of pitching or plunging airfoil oscillations.

In various cases summarized in Figs. 20-23, it is seen that the magnitudes of the lift and pitching moment decrease significantly and monotonically with increasing gust frequency. This might be expected from the well-known trends of the linear case, but it is very different from the effect of oscillatory airfoil motion. For pitching or plunging oscillations in transonic flow, the air loads typically decrease in magnitude with increasing frequency at low values of the reduced frequency k, but increase with frequency at higher values of k. However, the limiting low-frequency behavior of all three becomes the same as $k \to 0$.

B. Combined Gusts and Control-Surface Motions

A number of calculations were performed to examine the possibility of canceling gust-induced unsteady air loads by the appropriate motion of a simple trailing-edge flap, using the combined capability of the original LTRAN2 code and the present modifications for calculating gust response. The procedure is indicated schematically in Fig. 24. For example, if the problem were linear and the gust were described by Eq. (13), then the fluctuating lift due to the gust could be canceled by deflecting the flap as follows:

$$\delta_F = A \sin(t - \Theta) \tag{14}$$

where $A = G/F$; $\Theta = \theta_G - \theta_F$; G and θ_G are the magnitude and phase of the unsteady lift due to the gust but without flap deflections; and F and θ_F are the magnitude and phase of the unsteady lift caused by a small flap deflection (e.g., 1°), and reduced frequency k_G in a uniform oncoming flow. In other words, the principle of linear superposition could be used to determine the requisite flap deflection.

In the nonlinear, transonic case, however, the foregoing strategy would not be expected to work unless the gust were weak and the shock-wave motion in response to the gust were negligible. The cases depicted in Figs. 20-22, for example, do not satisfy these requirements. Consequently, when Eq. (14) was implemented for these conditions of M_∞ and k_G, substantial unsteady air loads remained, both C_L and C_M.

However, it was found that one additional iteration of the preceding strategy was adequate, that is, by employing the following flap deflection:

$$\delta_F = A_1 \sin(t + \Theta_1) + A_2 \sin(t + \Theta_2) \tag{15}$$

where

$$A_i = G_i/F$$

$$\Theta_i = \theta_{G_i} - \theta_F$$

$$i = 1,2$$

First, a calculation was done using Eq. (14) to specify the amplitude A_1 and phase Θ_1. Then the resulting response, G_2 and θ_{G_2} were used in a second calculation to determine $A_2 = G_2/F$ and $\Theta_2 = \theta_{G_2} - \theta_F$. For an example corresponding to the conditions of Fig. 21, this procedure reduced the magnitude of the unsteady lift coefficient from 0.080 with no flap deflection to 0.002. The resultant pressure distributions are shown in Fig. 25 in harmonic format. In particular, the in-phase component of C_p shows one spike centered on the mean shock-wave position and another near the hinge point of the flap.

Figure 25 also shows that even though the lift was essentially canceled, the pressure fluctuations remained large; and, in fact, a significantly larger pitching moment was developed with flap oscillation than without. Conversely, applying the strategy of Eq. (15) to minimize the pitching moments virtually canceled C_M, but at the expense of large fluctuating lift. A similar perversity, but of a somewhat lesser degree, was found by Ballhaus and Goorjian[21] in their attempts to cancel the effects of plunging motion with flap deflection; they showed that a combination of leading- and trailing-edge flaps was required to cancel both C_L and C_M. The basic problem in both cases is that the trailing-edge flap deflection produces an aft loading on the airfoil, whereas the loading resulting from a gust or from plunging oscillations tends to be effectively centered much closer to the quarter chord, $x = 0.25$. Therefore, it seems to be inherently impossible to provide effective active control of gust response with a simple trailing-edge flap. On the other hand, the present computational capability provides a new tool with which other gust-alleviation schemes can be studied.

V. Summary and Conclusions

Relatively straightforward modifications and improvements have been made in the computer code LTRAN2 that permit new classes of unsteady transonic-flow problems to be solved efficiently. Test cases have validated the new code, and sample results illustrate the essential effects of convected disturbances, both distributed and concentrated, on the flow in the vicinity of an airfoil.

The calculated results for discrete vortex-airfoil interactions show major distortions in the flow field as the vortex passes by. The most important factor in producing these distortions seems to be the time- and space-dependent vertical velocity, or local downwash and upwash, that is induced by the moving vortex, although its horizontal induced-velocity component also contributes in transonic cases. For vortex trajectories passing close to the airfoil, it is important to allow the vortex to move along a force-free path.

The time histories of the airloads that were obtained by running the code in the linear mode were somewhat similar, qualitatively, to the transonic results, even though the instantaneous chordwise pressure distributions were significantly different. Also, the maximum rates of change of the linear pressure results were significantly less.

In the case of a thin profile with a small leading-edge radius, large and rapidly varying pressure fluctuations were found to occur near the lower-surface leading edge. Since this is the region in which the small-disturbance approximation breaks down, the present results should be checked with a more accurate formulation.

The capability of the code to treat distributed vortical disturbances in the free stream was demonstrated for the case of a sinusoidal gust of vertical velocity. Again, the trends of the transonic results were qualitatively similar to the predictions of linear theory, but important quantitative differences were found, as would be expected, when the shock waves on the airfoils moved fore and aft.

Combined gust response and oscillating control surfaces were also examined, and a simple strategy was developed for suppressing the gust-induced air loads by activating a trailing-edge flap. However, the chordwise pressure distributions associated with gusts are very different from those produced by trailing-edge flap oscillations. Consequently, this simple approach cannot cancel both the gust-induced fluctuating lift and the pitching moments, even though one or the other can be suppressed almost completely by oscillating the flap with the proper phase and amplitude.

References

[1]Symposium on Aerodynamics of Vortical-Type Flows in Three Dimensions, AGARD Conference Proceedings CP-342, 1983.

[2]George, A. R. and Chang, S. B., "Noise Due to Transonic Blade-Vortex Interactions," American Helicopter Society Paper A-83-39-50-D000, May 1983.

[3]Ballhaus, W. F. and Goorjian, P. M., "Implicit Finite-Difference Computations of Unsteady Transonic Flows about Airfoils," AIAA Journal, Vol. 15, No. 12, Dec. 1977, pp. 1728-1735.

[4]Hessenius, K. A. and Goorjian, P. M., "Validation of LTRAN2-HI by Comparison with Unsteady Transonic Experiment," AIAA Journal, Vol. 20, No. 5, May 1982, pp. 731-732.

[5]Spreiter, J. R. and Alksne, A. Y., "Thin Airfoil Theory Based on Approximate Solution of the Transonic Flow Equation," NACA Report 1359, 1958.

[6]Van der Vooren, J., Slooff, J. W., Huizing, G. H., and van Essen, A., "Remarks on the Suitability of Various Transonic Small Perturbation Equations to Describe Three-Dimensional Transonic Flow — Examples of Computations Using a Fully Conservative Rotated Differencing Scheme," IUTAM Symposium Transsonicum II, K. Oswatitsch and D. Rues, Eds., Springer-Verlag, Berlin, 1976, pp. 557-566.

[7]Goorjian, P. M. and Van Buskirk, R., "Implicit Calculations of Transonic Flows Using Monotone Methods," AIAA Paper 81-0331, 1981.

[8]Caradonna, F. X., "The Transonic Flow on a Helicopter Rotor," Ph.D. Dissertation, Stanford University, Mar. 1978.

[9]Caradonna, F. X., Desopper, A., and Tung, C., "Finite-Difference Modeling of Rotor Flows Including Wake Effects," NASA TM-84280, 1982.

[10]Murman, E. M. and Stremel, P. M., "A Vortex Wake Capturing Method for Potential Flow Calculations," AIAA Paper 82-0947, 1982.

[11]Baker, G. R., "The 'Cloud in Cell' Technique Applied to the Rollup of Vortex Sheets," Journal of Computational Physics, Vol. 31, 1979, pp. 76-95.

[12]Steinhoff, J., "The Treatment of Convected Vortices in Compressible Potential Flow," Paper No. 22, Symposium on Aerodynamics of Vortical-Type Flows in Three Dimensions, AGARD CP-342, 1983.

[13]Goldstein, M. E., "Unsteady Vortical and Entropic Distortions of Potential Flows around Arbitrary Obstacles," Journal of Fluid Mechanics, Vol. 89, Pt. 3, 1978, pp. 433-468.

[14]Kerschen, E. J. and Myers, M. R., "Incidence Angle Effects on Convected Airfoil Noise," AIAA Paper 83-0765, 1983.

[15]Parathasarathy, R., "Aerodynamic Sound Generation Due to Vortex-Airfoil Interaction," Ph.D. Dissertation, Stanford U., Sept. 1972.

[16]Chow, C.-Y. and Huang, M.-K., "Unsteady Flows about a Joukowski Airfoil in the Presence of Moving Vortices," AIAA Paper 83-0129, 1983.

[17]Tijdeman, H., "Transonic Flow Past Oscillating Airfoils," Annual Review of Fluid Mechanics, Vol. 12, 1980, pp. 181-222.

[18]Sears, W. R., "Some Aspects of Non-Stationary Airfoil Theory and Its Practical Application," Journal of Aerospace Sciences, Vol. 8, No. 3, Mar. 1941, pp. 104-108.

[19]Graham, J. M. R., "Similarity Rules for Thin Airfoils in Non-Stationary Subsonic Flows," Journal of Fluid Mechanics, Vol. 43, Pt. 4, 1970, pp. 753-766.

[20]McCroskey, W. J., "Unsteady Airfoils," Annual Review of Fluid Mechanics, Vol. 14, 1982, pp. 285-311.

[21]Ballhaus, W. F. and Goorjian, P. M., "Unsteady Force and Moment Alleviation in Transonic Flow," Paper No. 14, Symposium on Unsteady Aerodynamics, AGARD Conference Proceedings CP-277, 1978.

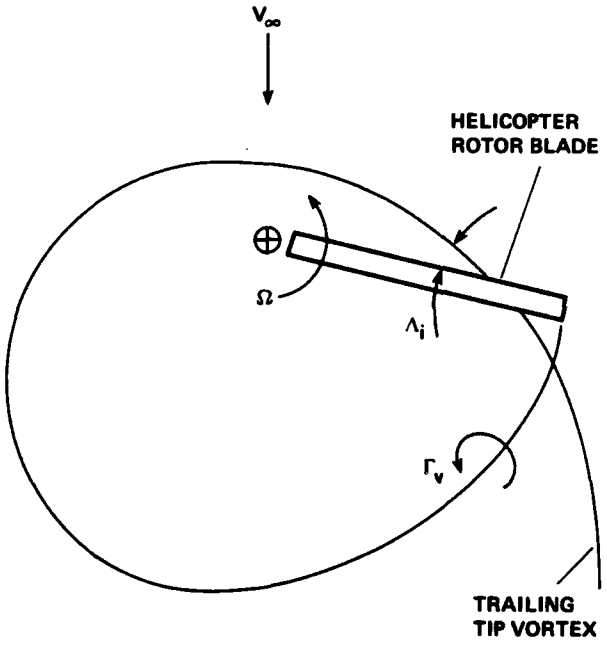

Fig. 1 Sketch of helicopter-rotor blade/vortex interaction.

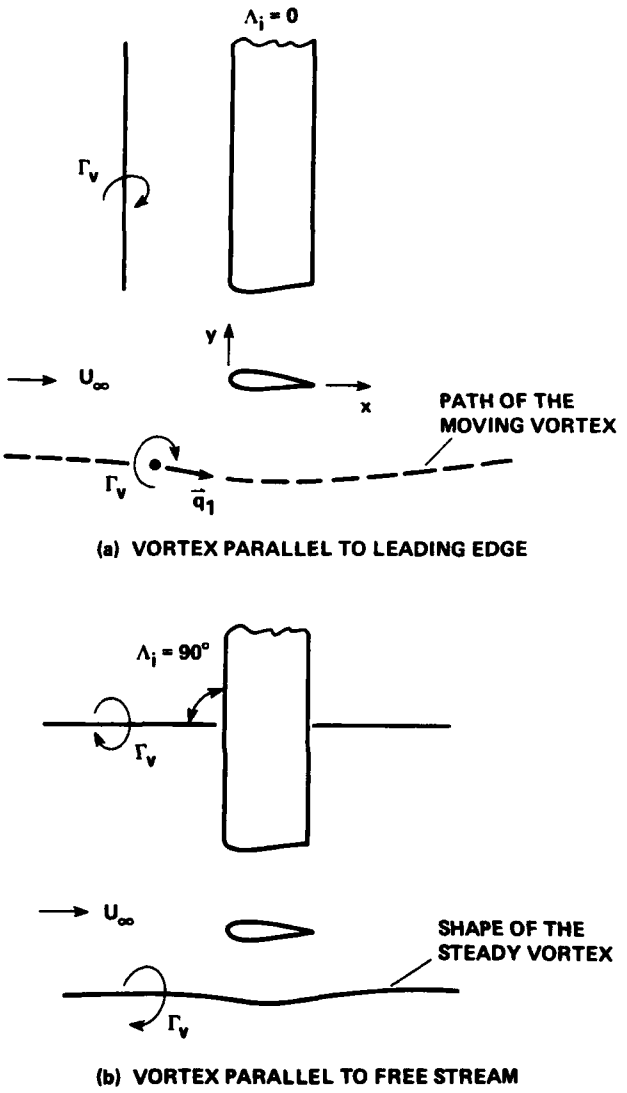

Fig. 2 Limiting cases of blade-vortex interaction.

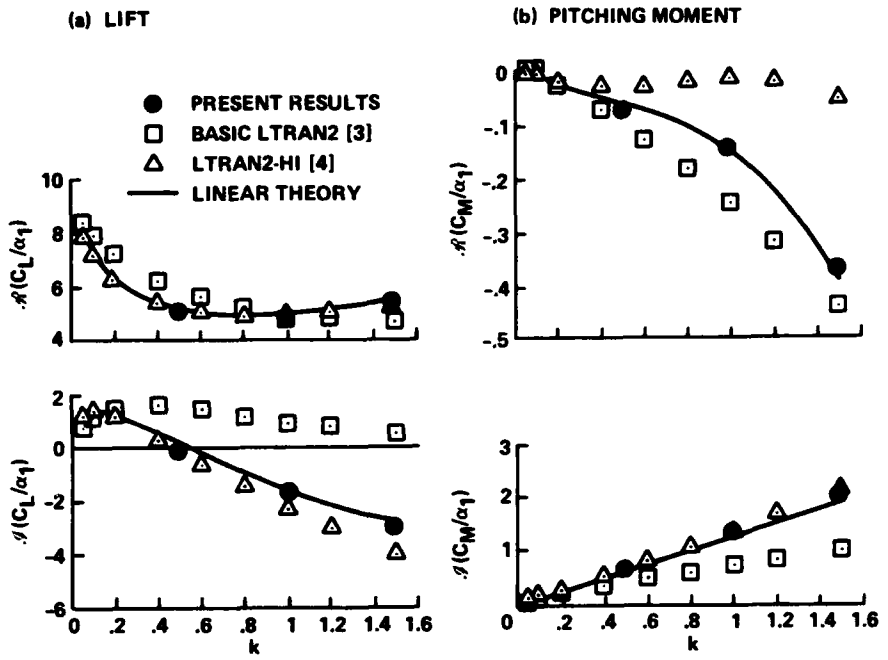

Fig. 3 Real and imaginary components of lift and pitching-moment coefficients for an airfoil oscillating in pitch at $M_\infty = 0.7$, $\alpha = \alpha_1 \sin \omega t$.

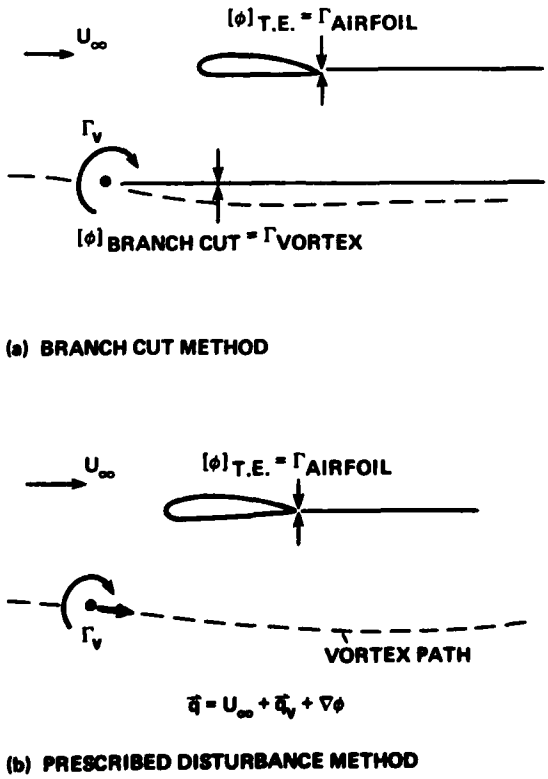

Fig. 4 Two methods for introducing the vortex.

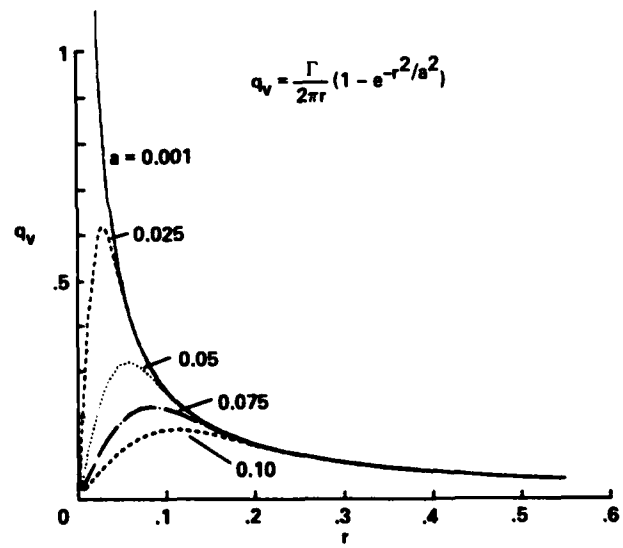

Fig. 5 The effect of core radius on the vortex-induced velocity field.

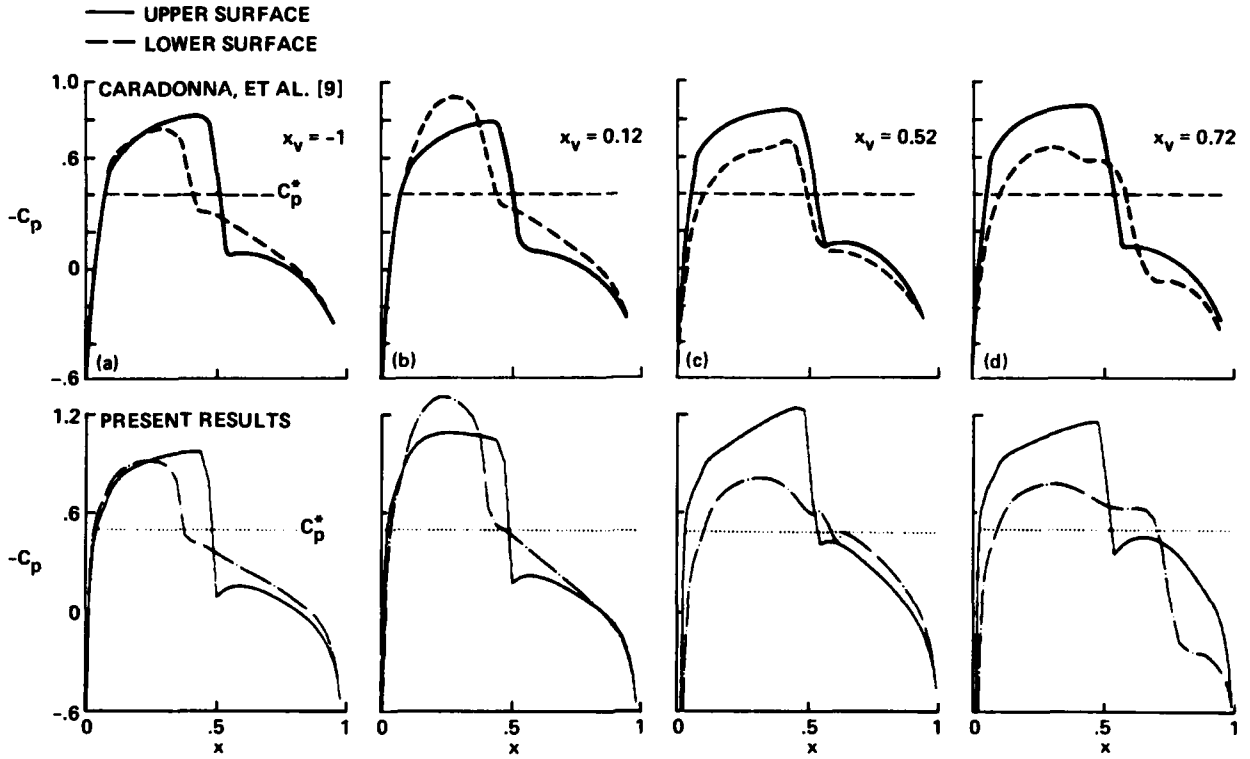

Fig. 6 Instantaneous pressure distributions during an airfoil-vortex interaction: NACA 0012 airfoil, $M_\infty = 0.80$, $\alpha = 0.5°$, $\Gamma = 0.20$, $y_v = -0.26$.

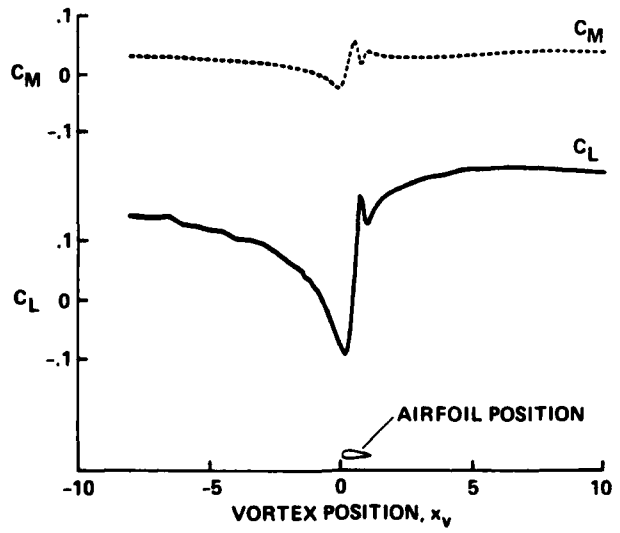

Fig. 7 Lift and pitching-moment variations versus instantaneous x-position of the vortex; same conditions as in Fig. 6.

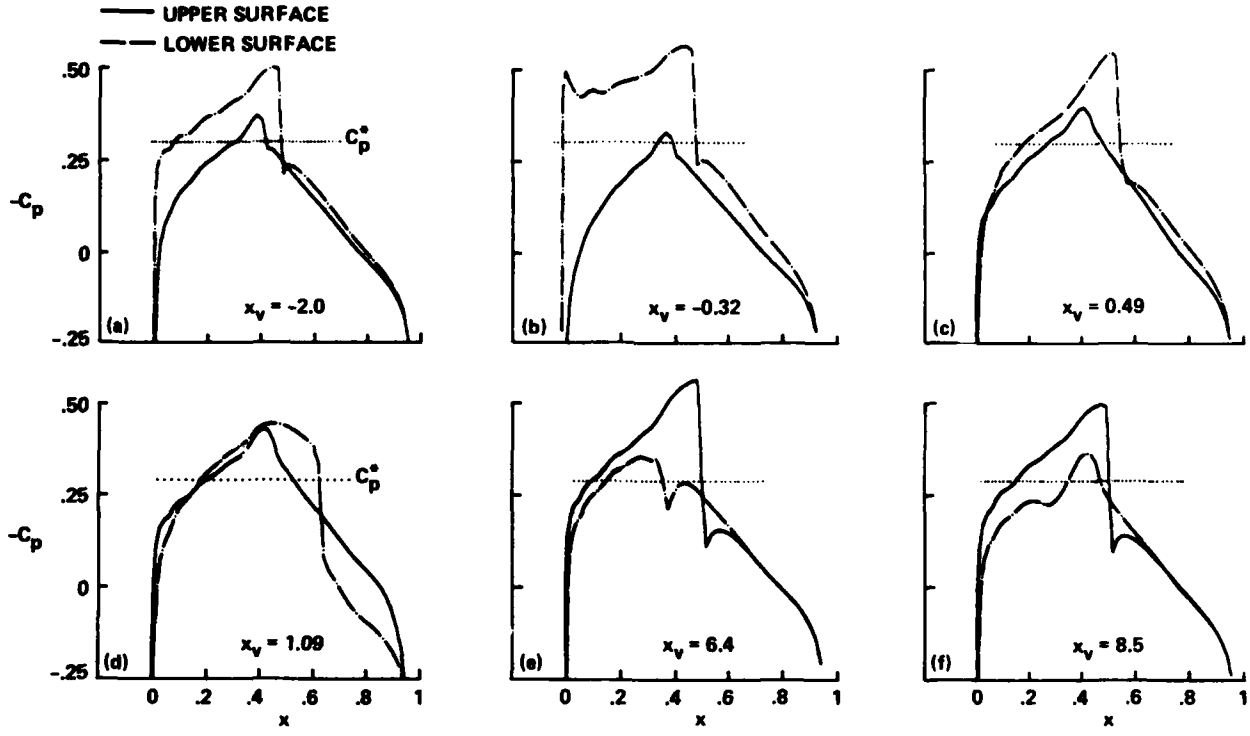

Fig. 8 Instantaneous pressure distributions during an airfoil-vortex interaction: NACA 64A006 airfoil, $M_\infty = 0.85$, $\alpha = 0$, $\Gamma = 0.20$, $y_{v_o} = -0.26$.

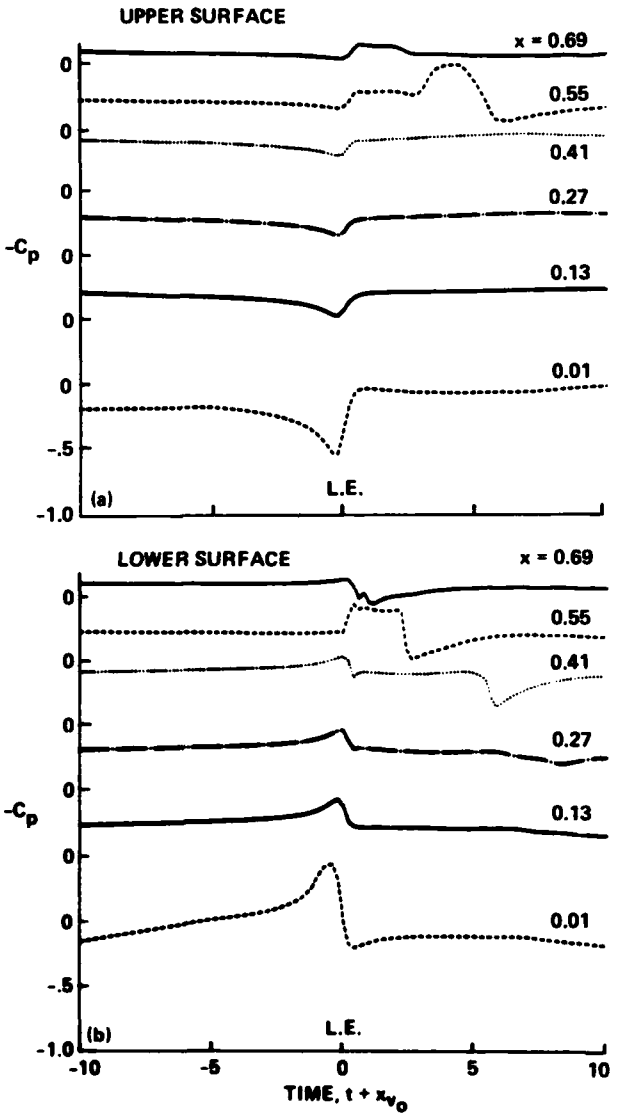

Fig. 9 Time histories of surface pressures for the conditions of Fig. 8.

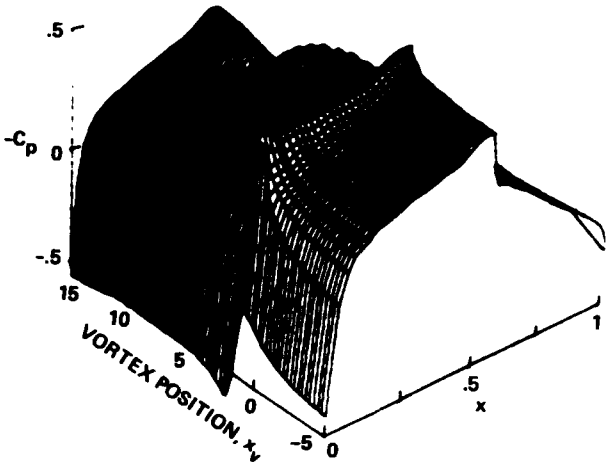

Fig. 10 Lower-surface pressure distributions on the NACA 64A006 airfoil for the conditions of Fig. 8.

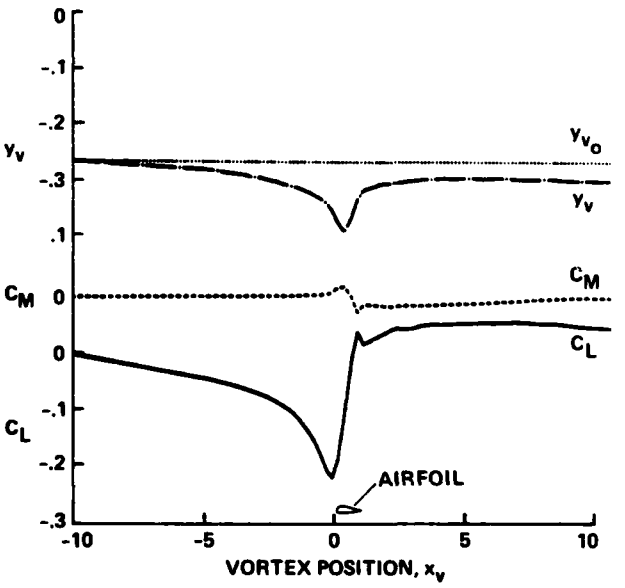

Fig. 11 Lift, pitching moment, and vortex displacement for the conditions of Fig. 8.

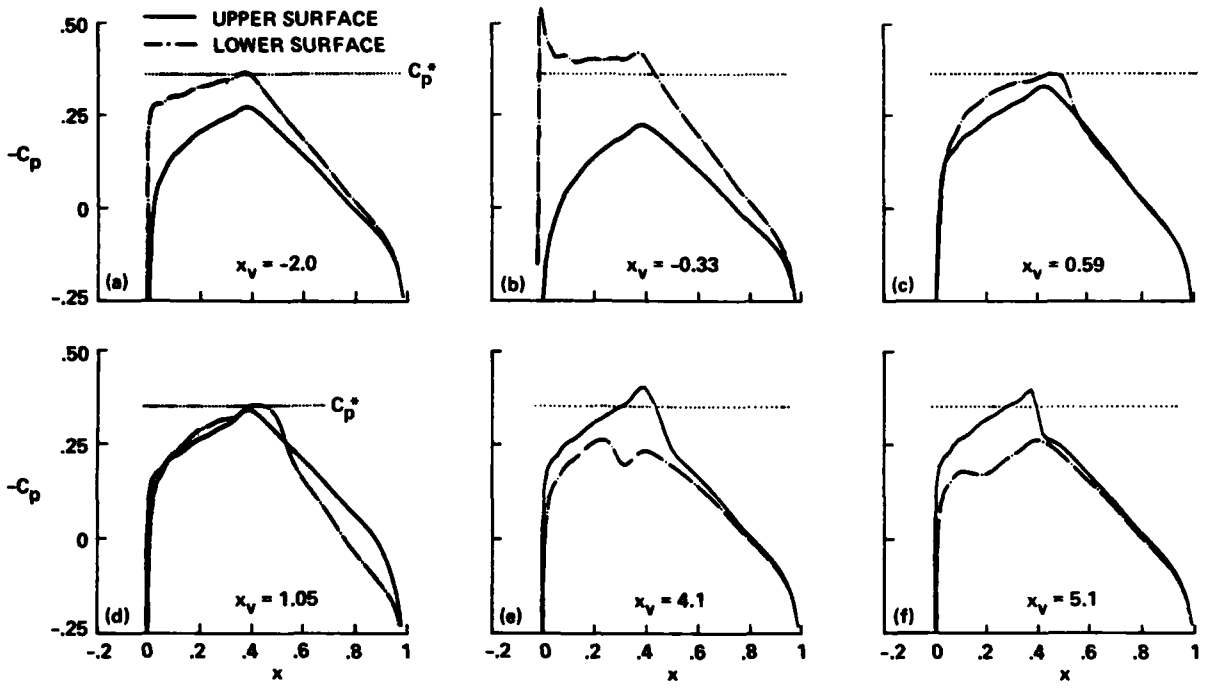

Fig. 12 Instantaneous pressure distributions during an airfoil-vortex interaction: NACA 64A006 airfoil, $M_\infty = 0.822$, $\alpha = 0$, $\Gamma = 0.20$, $y_{v_o} = -0.26$.

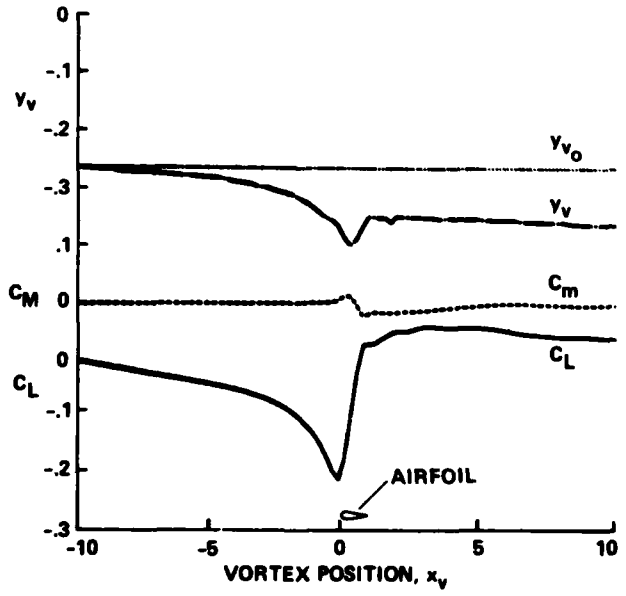

Fig. 13 Lift, pitching moment, and vortex displacement for the NACA 64A006 airfoil at $M_\infty = 0.822$.

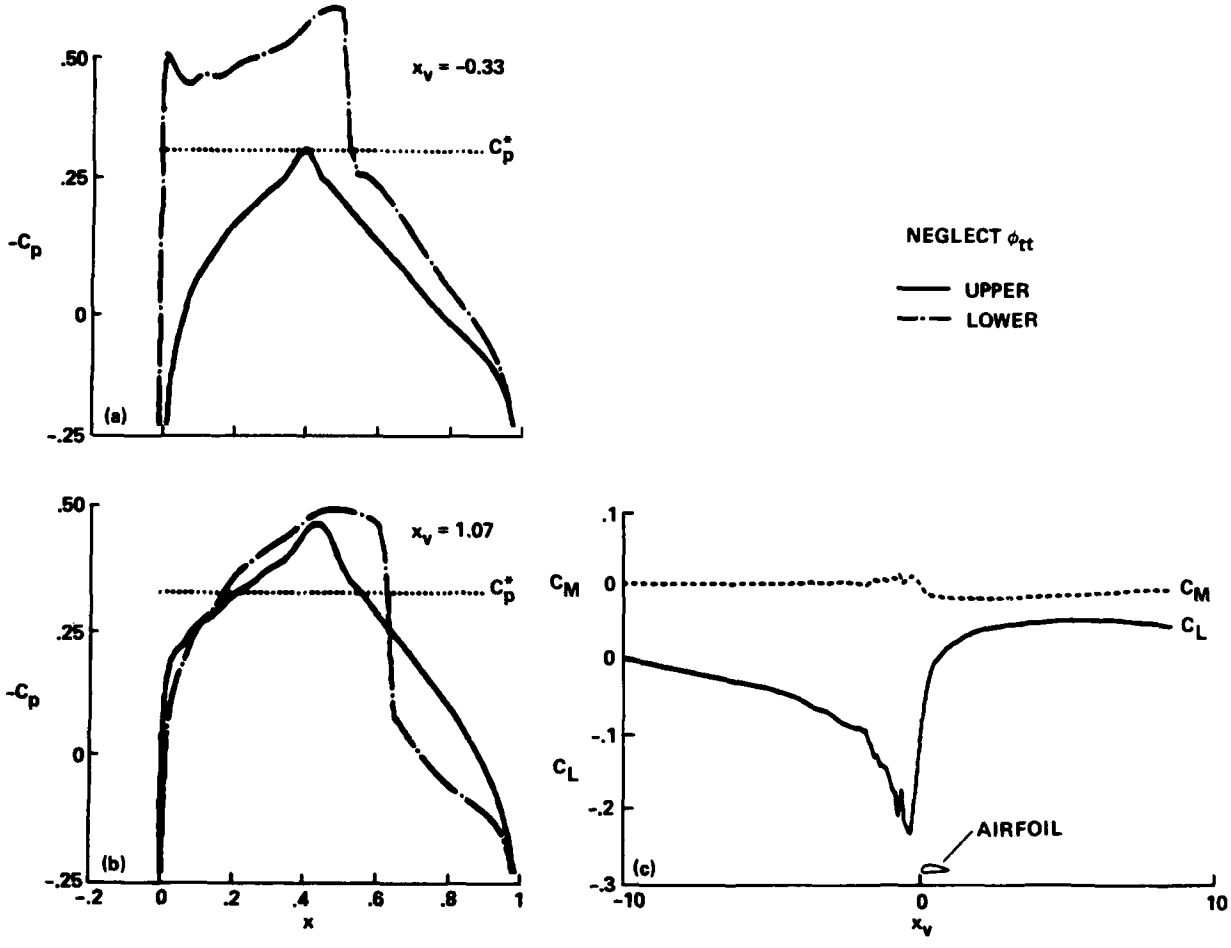

Fig. 14 The effect of neglecting ϕ_{tt}: NACA 64A006 airfoil, $M_\infty = 0.85$, $\alpha = 0$, $\Gamma = 0.20$, $y_{v_o} = -0.26$.

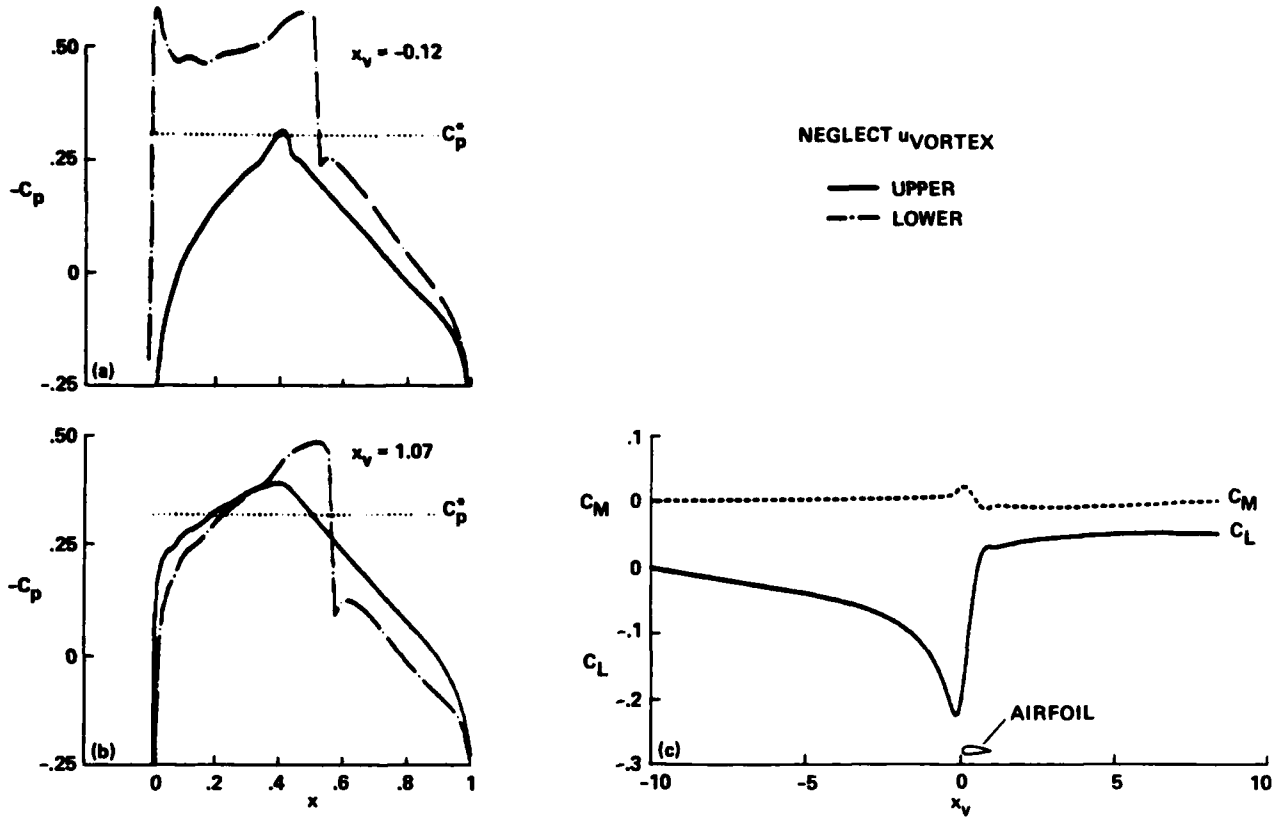

Fig. 15 The effect of neglecting u_v: NACA 64A006 airfoil, $M_\infty = 0.85$, $\alpha = 0$, $\Gamma = 0.20$, $y_{v_o} = -0.26$.

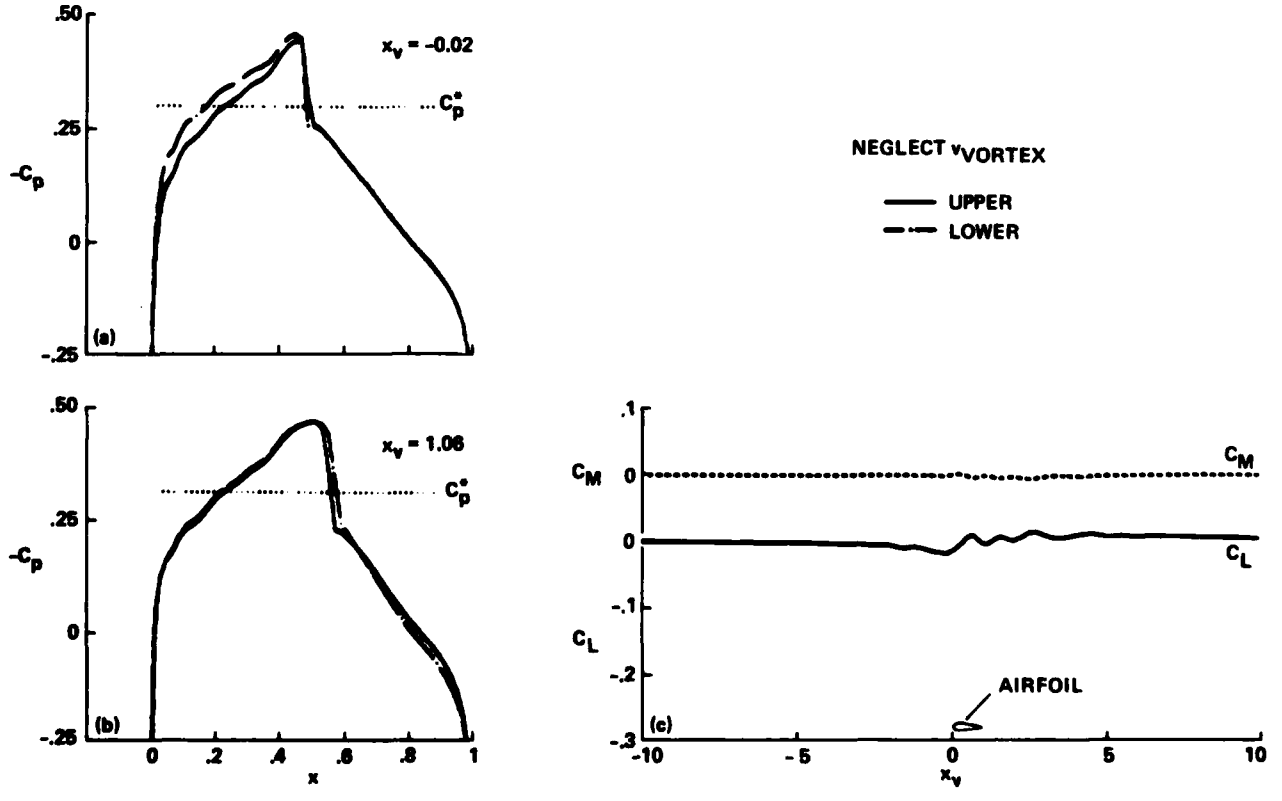

Fig. 16 The effect of neglecting v_v: NACA 64A006 airfoil, $M_\infty = 0.85$, $\alpha = 0$, $\Gamma = 0.20$, $y_{v_o} = -0.26$.

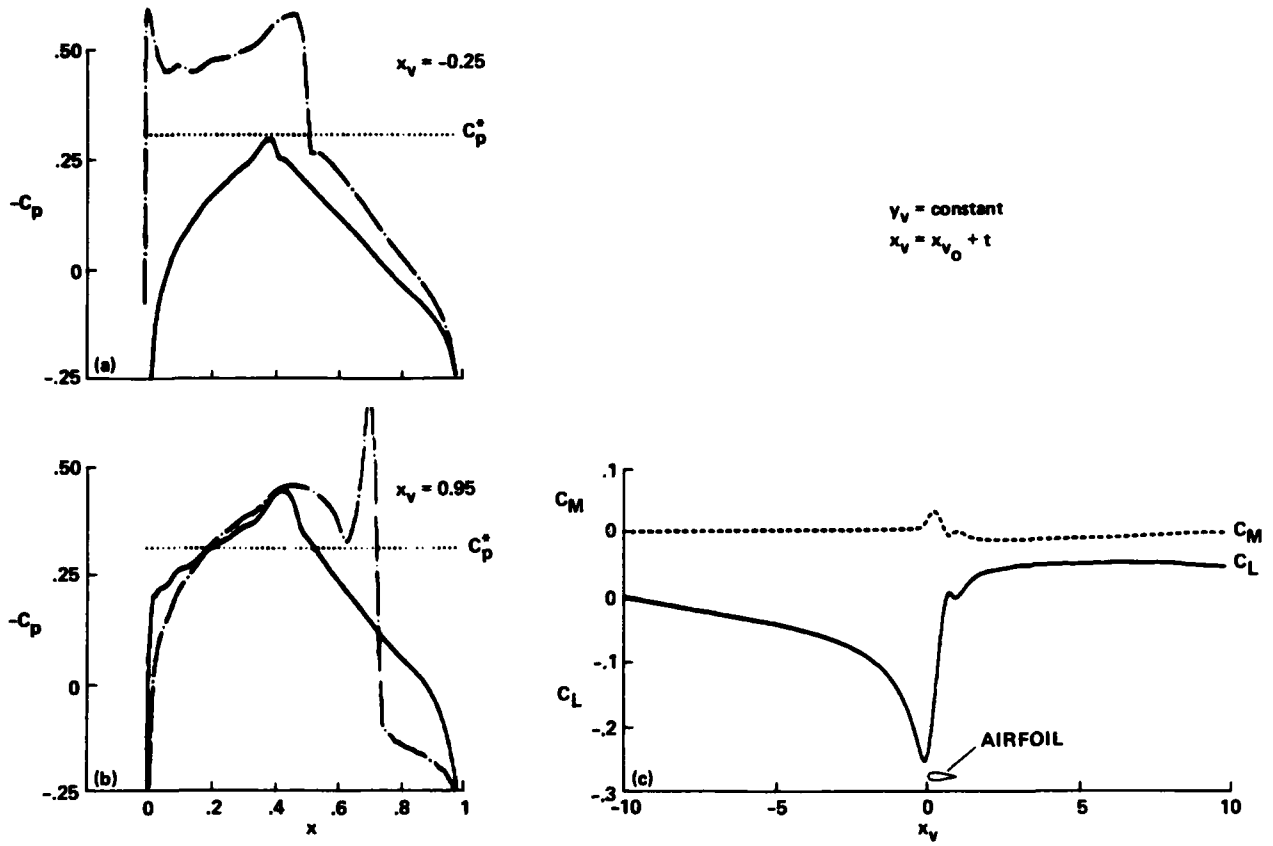

Fig. 17 The effect of specifying $y_v = y_{v_o}$: NACA 64A006 airfoil, $M_\infty = 0.85$, $\alpha = 0$, $\Gamma = 0.20$, $y_v = -0.26$.

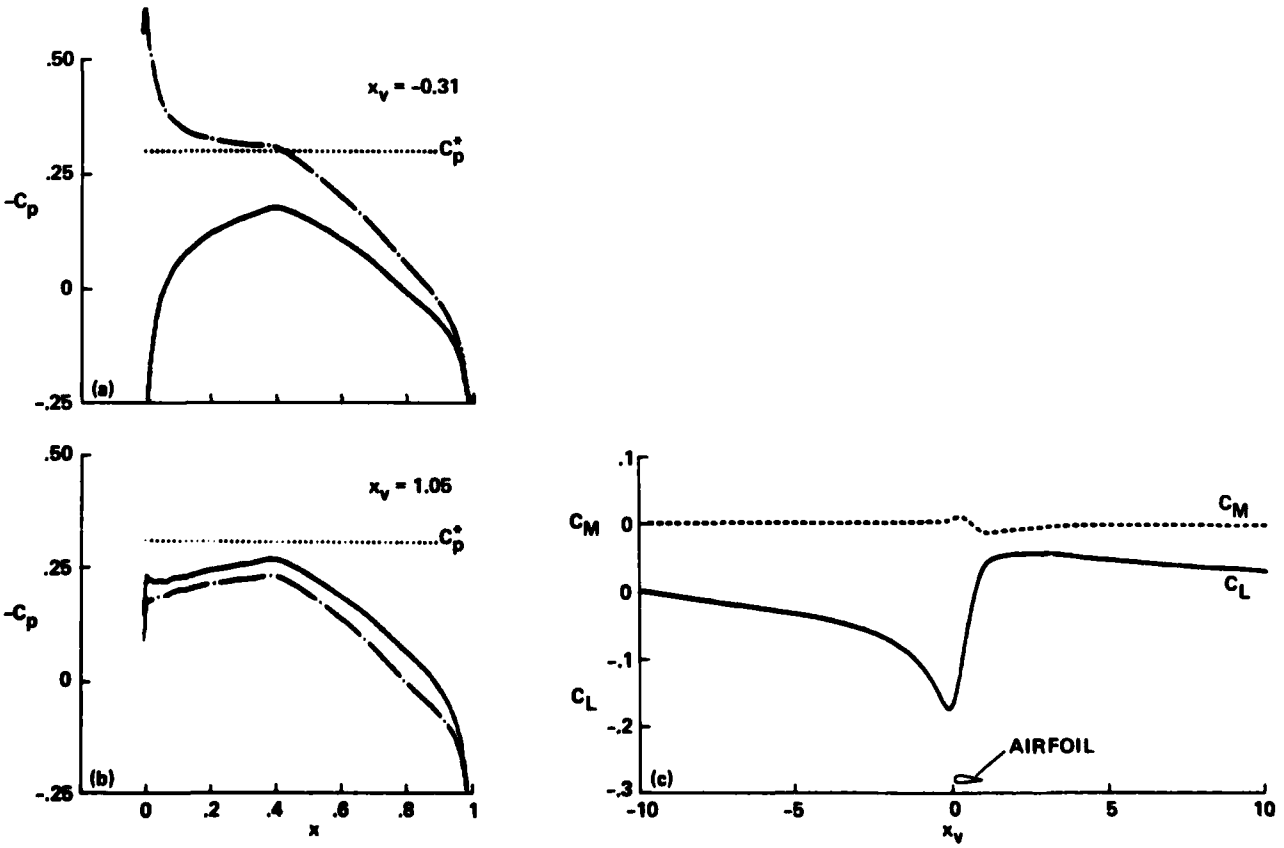

Fig. 18 Linear calculation: NACA 64A006 airfoil, $M_\infty = 0.85$, $\alpha = 0$, $\Gamma = 0.20$, $y_{v_o} = -0.26$.

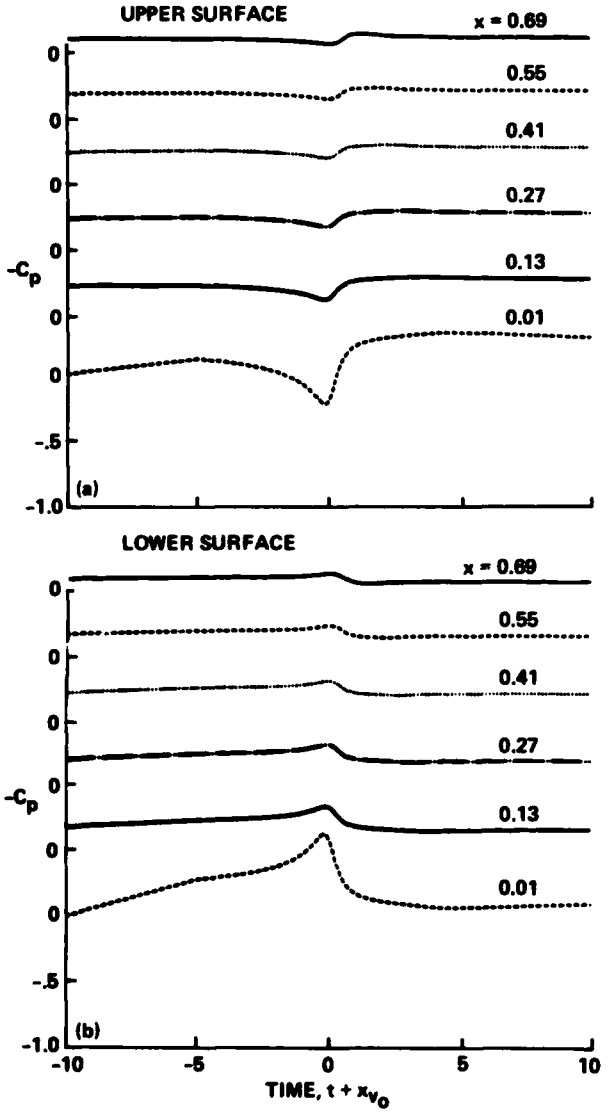

Fig. 19 Linear calculation of surface pressures.

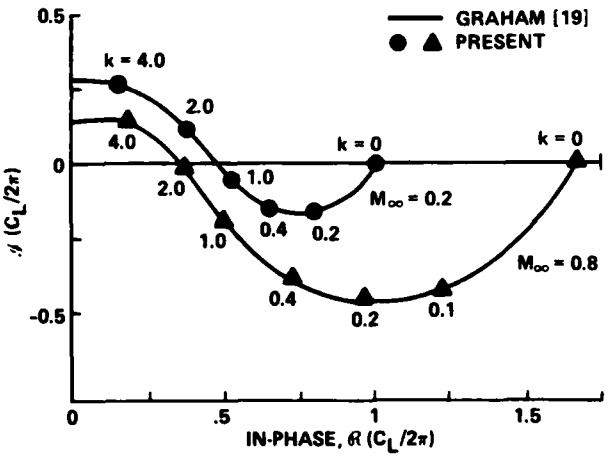

Fig. 20 Linear calculation of the lift response of an airfoil to a sinusoidal gust.

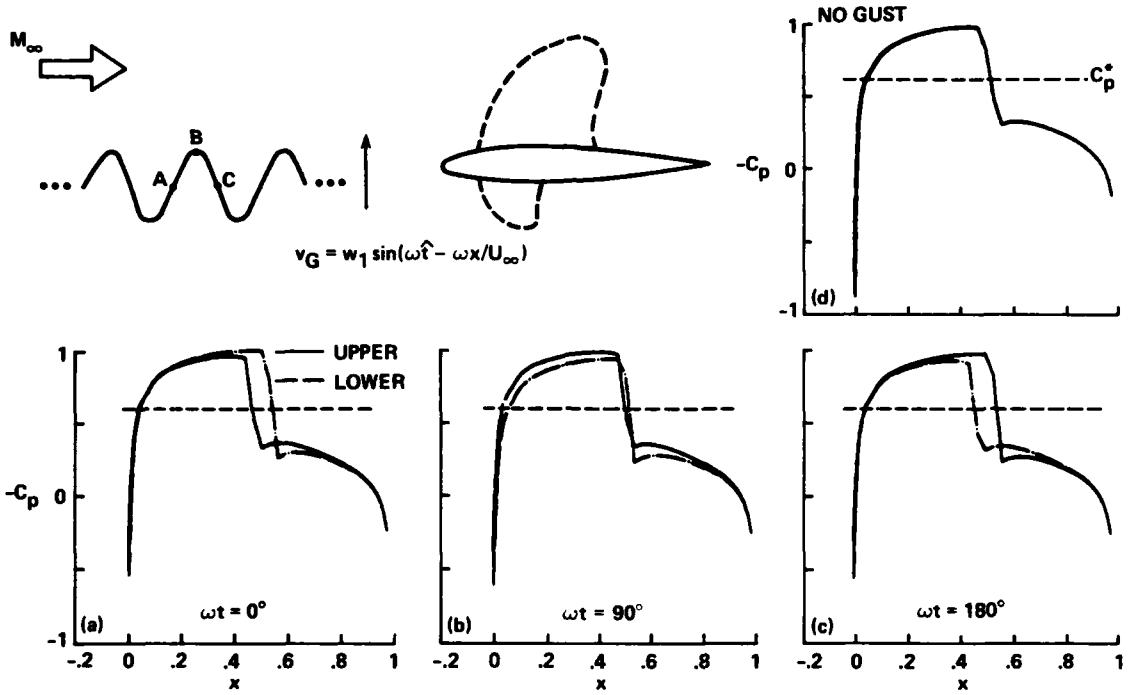

Fig. 21 Instantaneous pressure distributions due to a sinusoidal gust: NACA 0012 airfoil, $M_\infty = 0.80$, $\alpha = 0$, $k_G = 0.50$, $w_1 = 1°$.

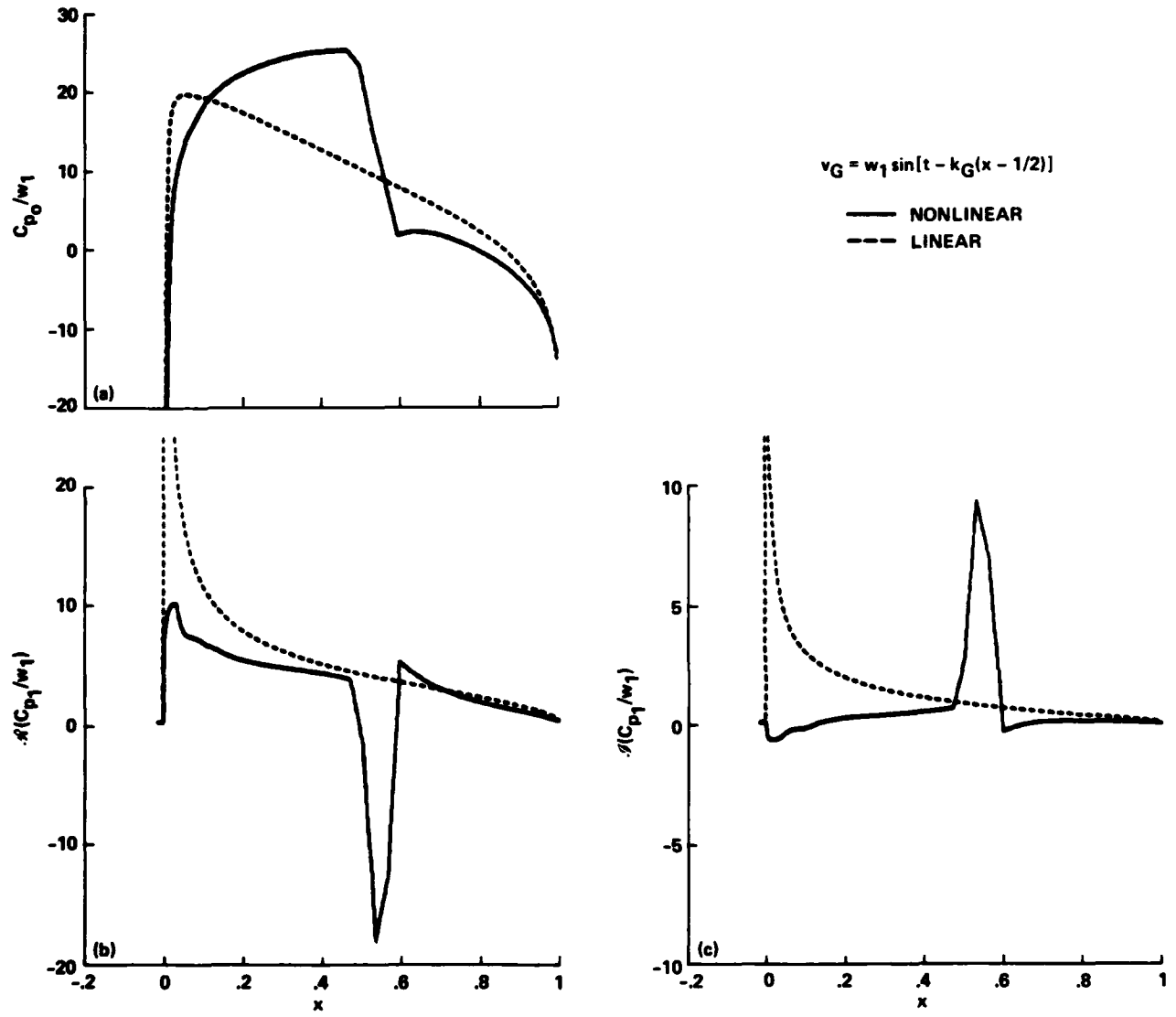

Fig. 22 Harmonic response of an NACA 0012 airfoil to a sinusoidal gust at $M_\infty = 0.80$, $k_G = 0.2$, $w_1 = 2°$.

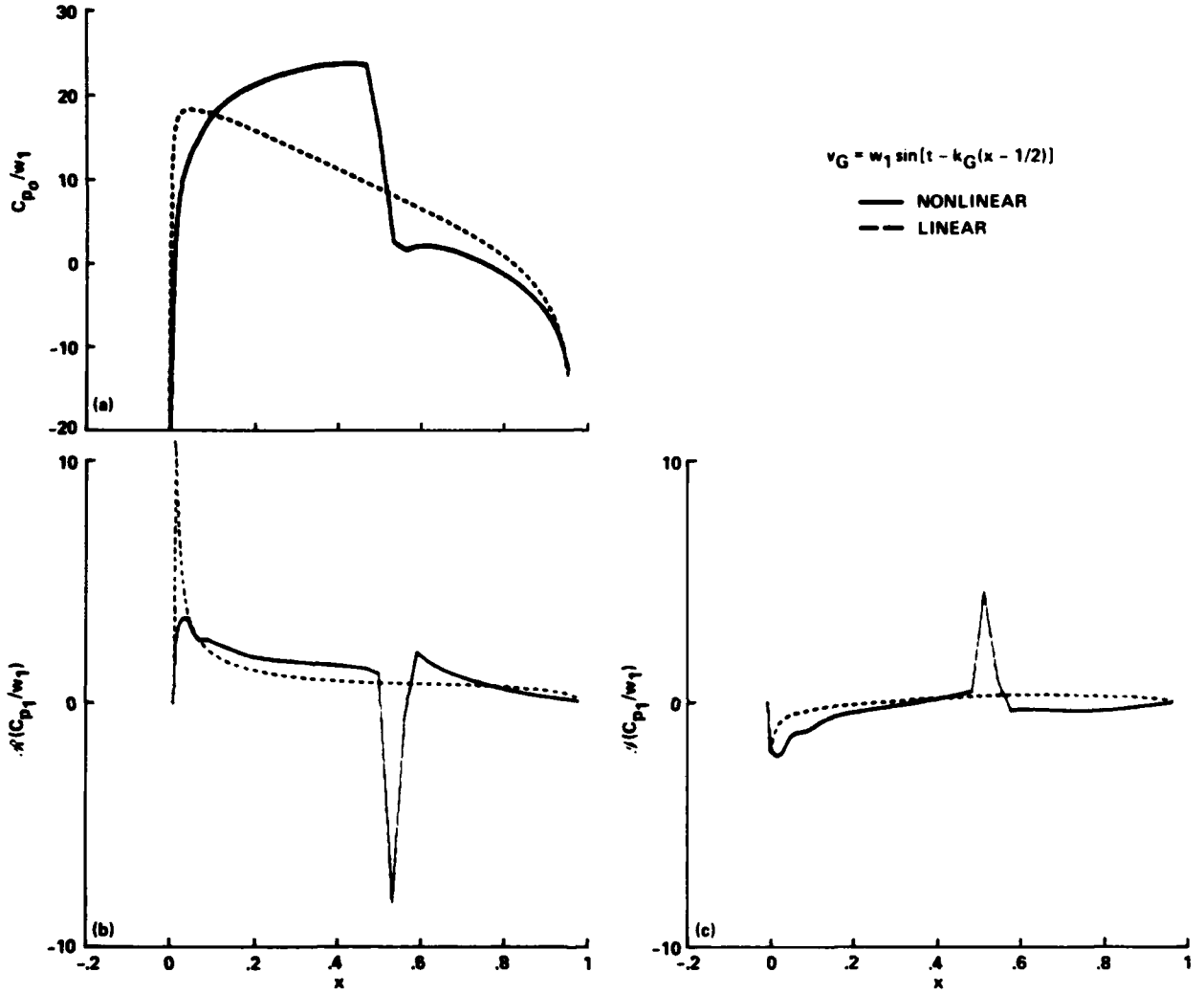

Fig. 23 Harmonic response of an NACA 0012 airfoil to a sinusoidal gust at $M_\infty = 0.80$, $k_G = 2.0$, $w_1 = 2°$.

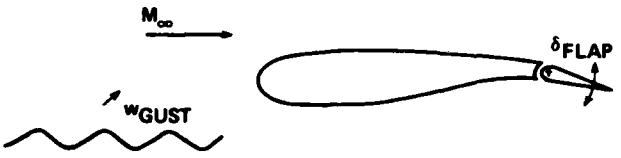

$w_G = fn(x, \hat{t})$ – SPECIFIED

$v_G = w_1 \sin(\omega_G \hat{t} - \omega_G c/U_\infty)$ – FIRST APPROXIMATION

$\delta_F = \delta_1 \sin(\omega_F \hat{t} + \theta)$

- ASSUME $\omega_F = \omega_G$
  DETERMINE δ_1 AND θ_F

Fig. 24 Alleviation of gust response by a trailing-edge flap.

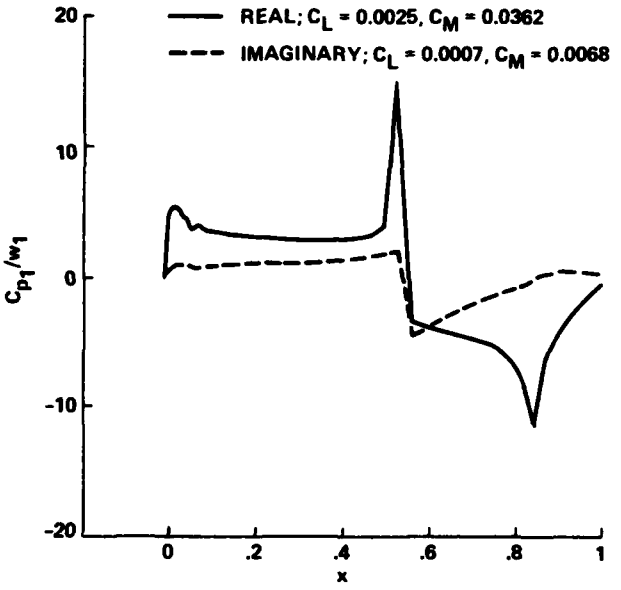

Fig. 25 Harmonic response for combined sinusoidal gust and flap deflection: NACA 0012 airfoil, $M = 0.80$, $k_G = 0.5$, $v_G = 1° \sin[\omega\hat{t} - k_G(x - 1/2)]$, $\delta_F = 2.56° \sin(\omega\hat{t} + 169°) + 0.60° \sin(\omega\hat{t} + 286°)$.

END

FILMED

11-83

DTIC